Color cone lasing emission in a dye-doped cholesteric liquid crystal with a single pitch

C.-R. Lee,[1,]* S.-H. Lin,[1] H.-C. Yeh,[1] T.-D. Ji,[1] K.-L. Lin,[1] T.-S. Mo,[2] C.-T. Kuo,[3] K.-Y. Lo,[4] S.-H. Chang,[1] Andy Y.-G. Fuh,[5,†] and S.-Y. Huang[6]

[1]*Institute of Electro-Optical Science and Engineering and Advanced Optoelectronic Technology Center, National Cheng Kung University, Tainan, Taiwan 701, Republic of China*
[2]*Department of Electronic Engineering, Kun Shan University of Technology, Tainan, Taiwan 710, Republic of China*
[3]*Department of Physics and Center for Nanoscience and Nanotechnology, National Sun Yat-sen University, Kaohsiung, Taiwan 804, Republic of China*
[4]*Department of Applied Physics and Institute of Optoelectronics and Solid State Electronics, National Chia Yi University, Chia Yi, Taiwan 600, Republic of China*
[5]*Department of Physics and Institute of Electro-optical Science and Engineering, National Cheng Kung University, Tainan, Taiwan 701, Republic of China*
[6]*Department of Optometry, Chung Shan Medical University, Taichung, Taiwan 402, Republic of China*
*Corresponding author: crlee@mail.ncku.edu.tw
[†]*Co-corresponding author: andyfuh@mail.ncku.edu.tw*

Abstract: This work investigates a novel color cone lasing emission (CCLE) based on a one-dimensional photonic crystal-like dye-doped cholesteric liquid crystal (DDCLC) film with a single pitch. The lasing wavelength in the CCLE is distributed continuously at 676.7–595.6 nm, as measured at a continuously increasing oblique angle relative to the helical axis of 0–50°. This work demonstrates that lasing wavelength coincides exactly with the wavelength at the long wavelength edge of the CLC reflection band at oblique angles of 0–50°. Simulation results of dispersion relations at different oblique angles using Berreman's 4×4 matrix method agrees closely with experimental results. Some unique and important features of the CCLE are identified and discussed.

©2009 Optical Society of America

OCIS codes: (230.3720) Liquid-crystal devices; (160.3710) Liquid crystals; (140.3600) Lasers, tunable; (140.3490) Lasers, distributed-feedback

References and links

1. E. Yablonovitch, "Inhibited Spontaneous Emission in Solid-State Physics and Electronics," Phys. Rev. Lett. **58**, 2059-2062 (1987).
2. S. John, "Strong localization of photons in certain disordered dielectric superlattices," Phys. Rev. Lett. **58**, 2486-2489 (1987).
3. E. Yablonovitch and T. J. Gmitter, "Photonic band structure: The face-centered-cubic case. Phys. Rev. Lett. **63**, 1950-1953 (1991).
4. E. Yablonovitch, T. J. Gmitter, R. D. Meade, A. M. Rappe, K. D. Brommer, and J. D. Joannopoulos, "Donor and acceptor modes in photonic band structure," Phys. Rev. Lett. **67**, 3380-3383 (1991).
5. J. P. Dowling, M. Scalora, M. J. Bloemer, and C. M. Bowden, "The photonic band edge laser: A new approach to gain enhancement," J. Appl. Phys. **75**, 1896-1899 (1994).
6. P. G. de Gennes and J. Prost, The Physics of Liquid Crystals (Oxford University Press, New York, 1993).
7. Y. Huang, Y. Zhou, Q. Hong, A. Rapaport, M. Bass, and S.-T. Wu, "Incident angle and polarization effects on the dye-doped cholesteric liquid crystal laser," Opt. Commun. **261**, 91-96 (2006).
8. D.-K. Yang and S.-T. Wu, Fundamentals of Liquid Crystal Devices (Wiley, Chichester, 2006).
9. K. Bjorknas, E. P. Raynes, and S. Gilmour, "Effects of molecular shape on the photoluminescence of dyes embedded in a chiral polymer with a photonic band gap," J. Mater. Sci.: Mater. Electron. **14**, 397-401 (2003).
10. V. I. Kopp, B. Fan, H. K. M. Vithana, and A. Z. Genack, "Low-threshold lasing at the edge of a photonic stop band in cholesteric liquid crystals," Opt. Lett. **23**, 1707-1709 (1998).
11. H. Finkelmann, S. T. Kim, A. Muñoz, P. Palffy-Muhoray, and B. Taheri, "Tunable mirrorless lasing in cholesteric liquid crystalline elastomers," Adv. Mater. **13**, 1069-1072 (2001).
12. J. Schmidtke, and W. Stille, "Fluorescence of a dye-doped cholesteric liquid crystal film in the region of the stop band: theory and experiment," Eur. Phys. J. B **31**, 179-194 (2003).

13. M. H. Song, N. Y. Ha, K. Amemiya, B. Park, Y. Takanishi, K. Ishikawa, J. W. Wu, S. Nishimura, T. Toyooka, and H. Takezoe, "Defect-mode lasing with lowered threshold in a three-layered hetero-cholesteric liquid-crystal structure," Adv. Mater. **18**, 193-197 (2006).
14. J. Schmidtke, W. Stille, H. Finkelmann, and S. T. Kim, "Laser emission in a dye doped cholesteric polymer network," Adv. Mater. **14**, 746-749 (2002).
15. Y. Zhou, Y. Huang, Z. Ge, L.-P. Chen, Q. Hong, Thomas X. Wu, and S.-T. Wu, "Enhanced photonic band edge laser emission in a cholesteric liquid crystal resonator," Phys. Rev. E **74**, 061705 (2006).
16. S. G. Lukishova, A. W. Schmid, A. J. McNamara, R. W. Boyd, C. R. Stroud, Jr., "Room temperature single-photon source: single-dye molecule fluorescence in liquid crystal host," IEEE J. of Selected Topics in Quantum Electronics **9**, 1512-1518 (2003).
17. S. G. Lukishova, A. W. Schmid, C. M. Supranowitz, N. Lippa, A. J. Mcnamara, R. W. Boyd, C. R. Stroud, Jr., "Dye-doped cholesteric-liquid-crystal room-temperature single photon source," J. of Modern Optics **51**, 1535-1547 (2004).
18. L. M. Blinov, G. Cipparrone, A. Mazzulla, P. Pagliusi, and V. V. Lazarev, "Lasing in cholesteric liquid cells: Competition of Bragg and leaky modes," J. Appl. Phys. **101**, 053104 (2007).
19. K. Dolgaleva, S. K. H. Wei, S. G. Lukishova, S. H. Chen, K. Schwertz, and R. W. Boyd, "Enhanced laser performance of cholesteric liquid crystals doped with oligofluorene dye," J. Opt. Soc. Am B **25**, 1496-1504 (2008).
20. A. Sugita, H. Takezoe, Y. Ouchi, A. Fukuda, E. Kuze and N. Goto, Numerical calculation of optical eigenmodes in cholesteric liquid crystals by 4×4 matrix method," J. Jpn. Appl. Phys. **21**, 1543-1546 (1982).

1. Introduction

Dielectric materials with sufficiently high periodic modulation of the refractive index have structures with photonic bandgaps [1-5]. The photons with wavelengths within such bandgaps are stopped from propagating inside photonic crystals (PCs) [1]. The bandgaps in PCs can markedly alter the fluorescence spectrum generated by excitation of doped active dyes; that is, fluorescence can be suppressed inside gaps and enhanced at band edges. Fluorescence can propagate via multi-reflection at band edges, resulting in a very slow group velocity and very large density of photonic state (DOS) for fluorescence [5]. Due to the distributed feedback of the active multilayer of a PC in the multi-reflection process, the rates of spontaneous and stimulated emissions at band edges are both enhanced, such that a high gain can be attained for a low-threshold lasing emission. Such PCs, consequently, can be used as mirrorless lasing resonators.

The cholesteric liquid crystal (CLC) has a large one-dimensional (1D) modulation of the refractive index, in which rod-like LC molecules assemble and rotate continuously along the helical axis, forming a so-called planar structure. Consequently, the planar CLC can be considered a PC with band gaps. Generally, two sets of optical eigenmodes (OEMs) with opposite handedness of circular polarization can exist within a CLC structure. Within these band gaps, the incident OEM component with the same handedness as the CLC helix can be entirely reflected, and another component with opposite handedness transmits entirely. Such a feature of selective reflection in the CLC within a certain band is described by the following equation [6,7]:

$$\lambda_C = n_{av}P\cos\phi, \qquad (1)$$

where λ_C is the wavelength at the band gap center in air, n_{av} is the average refractive index of the CLC, which satisfies the relation $n_{av}=[(n_e^2+n_o^2)/2]^{1/2}$ (n_e and n_o are the principal extraordinary and ordinary indices of refraction of the nematic host, respectively), P is helical pitch of the CLC, and ϕ is the refracted angle of the incident light entering the CLC with respect to the helical axis. Notably, ϕ is correlated with incident angle of light in air, θ, by Snell's law of $\sin\theta = n_{av}\sin\phi$ [7]. Furthermore, the photonic band structure of the CLC is also characterized by the following two equations for light propagation along the helical axis [8,9]:

$$\lambda_{\text{LWE}} = n_e \text{P}, \tag{2}$$

$$\lambda_{\text{SWE}} = n_o \text{P}, \tag{3}$$

where λ_{LWE} and λ_{SWE} are the wavelengths at the long- and short-wavelength edges (LWE and SWE), respectively, of the CLC reflection band (CLCRB).

Kopp *et al.* and others demonstrated that low-threshold lasing can occur at the edges of a CLCRB along the cell normal [10-19]. The fluorescence at the band edges of the CLCRB can reside in the CLC cavity over the long term, forming circularly polarized standing waves. When $n_e > n_o$, the optical fields of standing waves at the LWE and SWE of the CLCRB may rotate in directions parallel and perpendicular to the local director of the nematic host, respectively. Based on Fermi's Golden Rule, the rate of spontaneous emission, w_i, for ith OEM can be expressed by [12,13]

$$w_i = \rho_i \left| \mathbf{E}_i^* \cdot \boldsymbol{d} \right|^2 \tag{4}$$

where $\mathbf{E}_i$ and ρ_i are the optical field vector and DOS of the ith OEM, respectively, and $\boldsymbol{d}$ is the transition dipole moment vector of the active dye. This equation indicates that a good parallelism exists between $\boldsymbol{d}$ and $\mathbf{E}_i$ and a large ρ can enlarge w_i. Hence, the lasing emission at the LWE is typically stronger than that at the SWE since the optical field of the standing wave with λ_{LWE} and λ_{SWE} are on average parallel and perpendicular, respectively, to the molecular long axes and, thus, the local transition dipole moments of the dyes [14].

Based on Eq. (1), λ_C (and λ_{LWE} or λ_{SWE}) of the CLCRB for the incident light will continuously blue-shift when the angle of incidence, θ, increases continuously. We believe that the DDCLC lasing emission may generate along the nonzero oblique angle, that is, in the off-normal direction, with a conically symmetrical emission. This work, thus, reports for the first time an anomalous phenomenon, called color cone lasing emission (CCLE), based on a single-pitched 1D PC-like DDCLC cell. The lasing wavelength in the CCLE pattern is distributed continuously at 676.7–595.6 nm as the oblique angle increases continuously from 0° to 50° relative to the helical axis. The variation of the lasing wavelength in the CCLE with the oblique angle is consistent with that of the wavelength at the LWE of the CLCRB with the oblique angle. Simulation results obtained using Berreman's 4×4 matrix method show that, at each oblique angle, the associated group velocity and DOS are near zero and large at the SWE and LWE of the CLCRB, respectively, and are in good agreement with experimental results. The inhomogeneous angular distributions of the relative intensity and, thus, the energy threshold of the CCLE can be attributable to the angular dependences of the loss of fluorescence from the multi-reflection process and fluorescence spectrum of the spontaneous emission of laser dyes at the LWE.

2. Sample preparation and experimental setups

The nematic LC (NLC), left-handed chiral dopant and laser dye employed in this study are ZLI2293 (n_e=1.6312 and n_o=1.4990 at 20°C) (Merck), S811 (Merck) and 4-Dicyanmethylene-2-methyl-6-(p-dimethylaminostyryl)-4H-pyran (DCM) (Exciton), respectively. The mixing ratio of ZLI2293:S811 in the CLC mixture is 78:22 *wt%*. The concentration of DCM in the CLC mixture is 0.5*wt%*. Two indium-tin-oxide (ITO)-coated glass slides separated by two 25µm-thick plastic spacers are used to fabricate each empty cell. Both glass slides are pre-coated with polyvinyl alcohol (PVA) film, and rubbed in the same direction. Homogeneously mixed CLC compounds with DCM doping are then injected into the empty cell, forming a planar DDCLC cell. Before the lasing experiments, the DDCLC cell is placed in a clean, dark specimen box in the laboratory at room temperature for about 2 weeks, such that the CLC can slowly self-organize to a perfect planar structure.

This work utilizes two experimental setups, setups (i) and (ii) (Figs. 1(a) and 1(b)), for measuring the fluorescence (or lasing) emission spectrum and reflection spectrum of the DDCLC at each oblique angle, respectively. In Fig. 1(a), one pumped laser beam, derived from a Q-switched Nd:YAG second harmonic generation (SHG) pulse laser (wavelength: 532 nm) with a pulse duration of 8ns, repetition rate of 10Hz and pulse energy, E, is focused by lens L1 (focal length=20cm) on the DDCLC cell at an incident angle of $\alpha=10°$ relative to the cell normal (N) along the helical axis of the planar structure. The cell is fixed (cannot rotate). A fiber-optic probe of a fiber-based spectrometer (USB2000-UV-VIS) (Ocean Optics) is moved behind the cell along a quarter circular trajectory ($C_{1/4}$) with a radius R on the xy plane and the center of the pumped spot on the cell to record the fluorescence (or lasing) spectrum of the DDCLC at each oblique angle θ_1. Notably, θ_1 is defined as the oblique angle between N and the line extending from the fiber optic probe of the spectrometer to the pumped spot on the xy plane. A half-wave plate ($\lambda/2$ for 532 nm) and polarizing beam splitter (PBS) are placed in front of L1 for adjusting incident laser pulse energy. To analyze the measured fluorescence (or lasing) emission spectrum of the DDCLC cell at a particular oblique angle, the reflection spectrum of the same cell, which indicates the photonic band structure of the CLC, is also measured at that same oblique angle. In Fig. 1(b), one non-polarized white beam from an Hg lamp (300–750nm) is pre-collimated and passes through a diaphragm with an aperture of 0.5 cm in diameter to illuminate the DDCLC cell. The fiber-optic probe of the spectral measurement system is placed behind and near the cell to receive the white beam passing through the cell for measuring the reflection spectrum (complementary to the transmission spectrum) of the DDCLC cell at a particular oblique angle θ_2. Notably, θ_2, the angle between the incident direction of the white beam and N on the xy plane, can be altered by rotating of the cell around the z-axis.

(a)

(b)
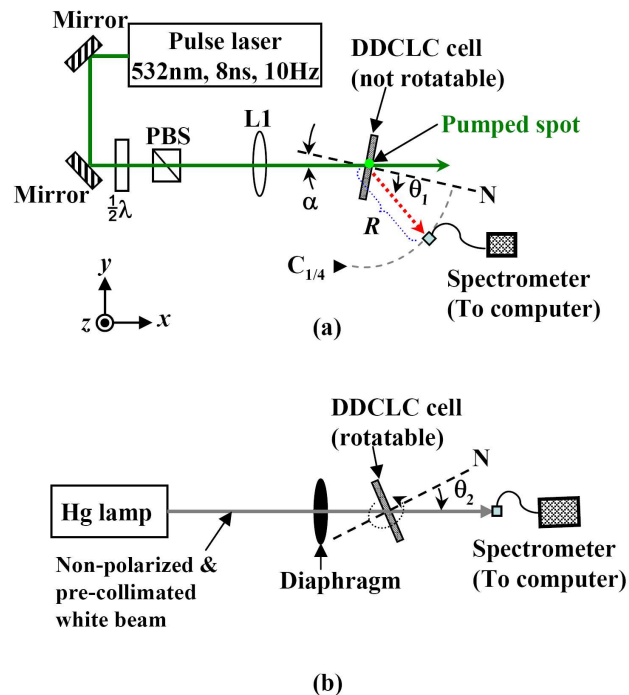
Fig. 1. Top views of Experimental setups for measuring (a) the fluorescence (or lasing) and (b) the reflection spectra of the dye-doped cholesteric liquid crystal (DDCLC) cell. N: cell normal; $\lambda/2$: half waveplate for 532nm; PBS: polarizing beam splitter; L1: lens; α: angle of incidence of the pumped pulses relative to N.

3. Results and discussion

One cone lasing pattern (Fig. 2(a)) can be generated instantly and appears on screens placed on both sides of the cell when the single-pitched DDCLC cell is excited by incident laser pulses with an energy of E=8.3μJ/pulse. Because the lasing emission is distributed conically and symmetrically about **N**, one can chose, without losing generality, to measure and study the features of lasing signals emitting in a reference plane crossing the cell plane and containing **N**, say, the *xy* plane, at different oblique angles θ_1. The lasing emission along **N** ($\theta_1=0°$) is called normal lasing. The fiber-optic probe is placed behind the cell and moves along $C_{1/4}$ with a radius *R* of roughly 2cm on the *xy* plane (Fig. 1(a)) to measure the angle-associated lasing signals and a distribution of lasing spectra (Fig. 2(b)) with a continuously blue-shifting lasing wavelength of 676.7 (black curve) to 595.6 nm (pink dotted curve) (roughly 81nm bandwidth) can be measured and identified by increasing the value of θ_1 from 0° to 50°. Although the lasing emissions occurred at angles not equal to either 0° or 35° all are weak and therefore cannot be observed easily (Fig. 2(a)); however, the sensitive spectrometer can still detect these lasing emissions easily (Fig. 2(b)). The full widths at half-maximum (FWHM) for these measured lasing signals emitting at different oblique angles are distributed at 0.5–2 nm. When the angle exceeds 50°, lasing is difficult to generate. Experimental results (will be presented in a forthcoming paper) indicate that the band of such a lasing emission can be tuned to encompass different color regions (e.g., from deep red region to light red, orange, yellow, or green region) distributed within a wide cone angle by changing the pitch of the DDCLC. This lasing effect is called the CCLE. This novel finding demonstrates that a "single pitched" DDCLC laser can simultaneously emit a wide banded lasing emission with an angular dependence on the wavelength. This contradicts the conventional belief that, at most, two lasing peaks at the two band edges can simultaneously occur in the normal direction in a DDCLC [10-19].
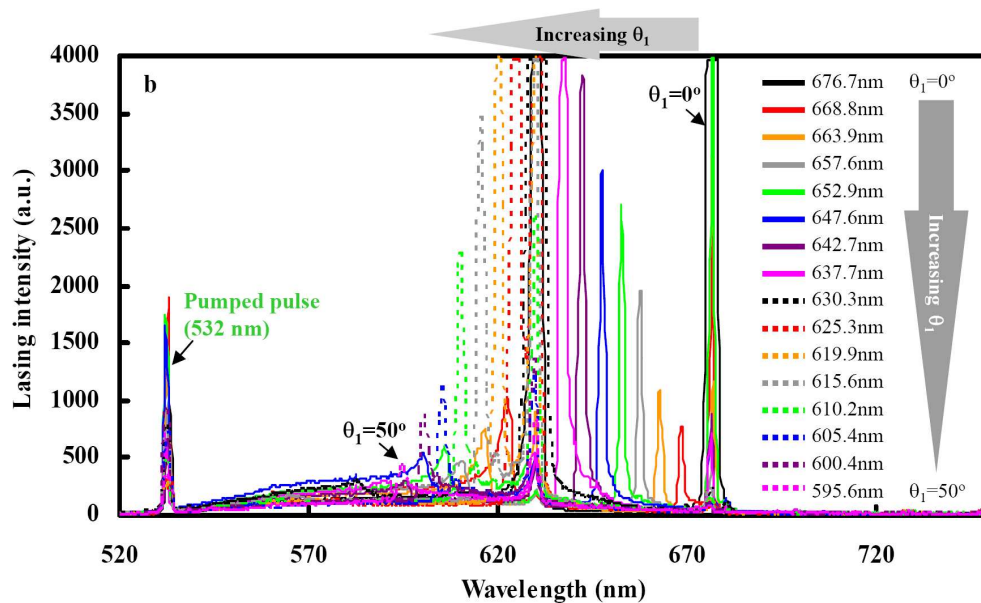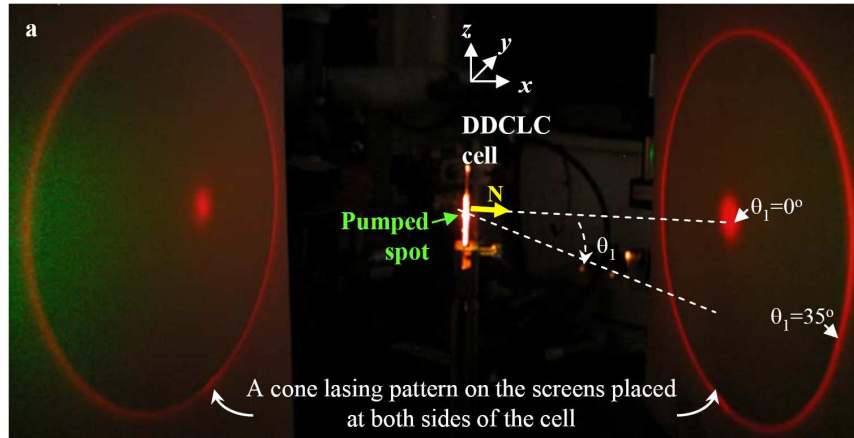
Fig. 2. (a) One CCLE pattern is generated instantly and presented on the screens placed at both sides of the cell after the cell is excited by the pumped pulses with energy 8.3μJ/pulse. (b) Obtained continuous distributions of the lasing spectra in CCLE measured at oblique angles relative to **N** continuously increasing from θ_1=0° to 50°.

To further analyze the CCLE, six lasing signals with different lasing wavelengths—λ_{las} = 676.7, 663.9, 642.7, 630.3, 619.9 and 600.4 nm—measured at θ_1=0°, 17°, 29°, 35°, 39° and 46°, respectively, in the lasing spectra (Fig. 2(b)) are chosen randomly. Additionally, six reflection spectra of the cell at these six corresponding oblique angles are measured and compared with the six lasing spectra obtained previously. Figure 3 shows comparison results; the curves with black, red, orange, pink, green, blue peaks (notches) represent, respectively, the lasing (reflection) spectra of the cell measured at θ_1 (θ_2) = 0°, 17°, 29°, 35°, 39° and 46°. The reflection and lasing spectra measured at 0° are also included in each subfigure (Fig. 3) for comparison with those measured at nonzero oblique angles. Clearly, a lasing peak exists at the LWE of the CLCRB at each oblique angle. These experimental results demonstrate that the lasing signal emitting at zero or nonzero oblique angles conform to the edge lasing theory

for distributed feedback resonators. This theory states that low-threshold lasing emissions can occur at band edges of a stop band. Notably, lasing can also be observed at the SWE of the CLCRB at $\theta_1 \le 17°$ (Figs. 2(b) and 3). However, lasing emissions at angles of $\theta_1 < 17°$ at the SWE are all much weaker than those at the LWE, with the exception of the strong lasing peak at the SWE at 0°. Because the CCLE effect at the LWE is much better than that at the SWE in this study, the following discussion focuses on the former. The lasing emissions at 0° and 35° are sufficiently strong and can be detected at some nonzero oblique angles due to their strong scattering (Fig. 3).
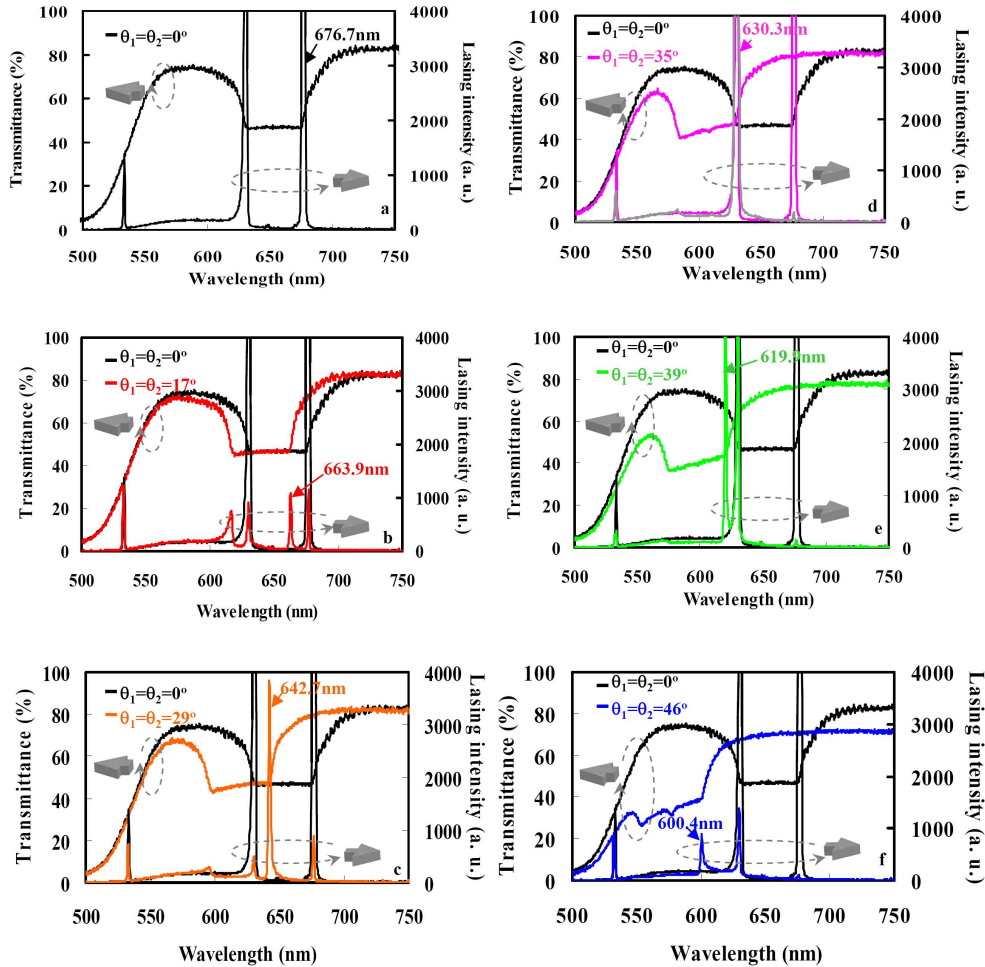
Fig. 3. Six lasing spectra measured at θ_1= (a) 0°, (b) 17°, (c) 29°, (d) 35°, (e) 39°, and (f) 46° are randomly selected from Fig. 2(b) and compared with reflection spectra measured at those six oblique angles θ_2 (=θ_1).

As demonstrated by Kopp *et al.* in identifying the low-threshold edge laser in DDCLC cells, the low-threshold lasing at the band edges of the CLC stop band is associated with the singularities at the edges in the DOS of OEMs propagating along the normal of the CLC multi-layer structure [10]. This high DOS can generate a slow group velocity, v_g, that approaches zero at the edges. The lifetime of OEMs at the edges is thereby prolonged, such that they obtain a gain needed for a low-threshold lasing. To prove that edge lasing theory can explain lasing emissions in the CCLE at the nonzero oblique angles, the dispersion relations for OEMs propagating at different oblique angles in a planar CLC are determined. Initial calculation using the commercially provided parameters of refractive indices of LC indicates

that the simulated CLCRB at the normal direction (0°) (not shown herein) is wider than the CLCRB measured at 0° (Fig. 3(a)); however, the central wavelengths of the two reflection bands are almost the same. The discrepancy in the width of the two CLCRB probably results from the decrease in the birefringence of the NLC after adding 22 *wt%* non-birefringent chiral dopant to the NLC host [15]. To obtain actual values of the principal extraordinary and ordinary refractive indices of the LC in the CLC, a separate calculation is pre-performed as follows. The value of the pitch, P, of the CLC obtained is approximately 417.55nm by substituting the values of measured λ_C and n_{av} ($=[(n_e^2+n_o^2)/2]^{1/2}$) into Eq. (1), in which the values of n_e and n_o are 1.6312 and 1.4990, respectively (obtained from Merck). Because lasing emissions occurred at the edges, the value of λ_C can be pre-obtained experimentally from the average value of λ_{lasing} at the LWE and SWE of the CLCRB (λ_{las}(LWE) and λ_{las}(SWE), respectively) at 0°. The actual values of the extraordinary and ordinary indices of 1.62065 and 1.50955, respectively, are obtained by substituting the obtained values of λ_{las}(LWE)=676.7nm and λ_{las}(SWE)=630.3nm at 0° and P=417.55nm into Eqs. (2) and (3). Then, all of these obtained parameter values are substituted into the following simulation of the dispersion relations in the planar CLC.

The propagation characteristics of OEMs at different oblique angles in a planar CLC can be examined by simulating the dispersion relation, $\omega_N(k_N)$, or equivalently, $k_N(\lambda)$, using Berreman's 4×4 matrix method [20], in which $k_N (\equiv k/(2\pi/P))$ and $\omega_N (\equiv \omega/(2\pi c/P))$ are defined as the normalized wave number and normalized angular frequency of OEMs, respectively, and λ is the wavelengths of OEMs. Simulation results for $\omega_N(k_N)$ and $k_N(\lambda)$ are within the wavelength range of 500–750 nm at the six oblique angles of incidence—$\theta=0°$, 17°, 29°, 35°, 39° and 46° (Figs. 4(a) and 4(b)). Obviously, four OEMs exist with particular wavelengths or angular frequencies at each oblique angle. Two OEMs with positive and negative real solutions of k_N (black curves in Fig. 4) can propagate in opposite directions without reflection in the planar CLC. However, the other two OEMs can be reflected entirely in opposite directions within the forbidden gap where the positive and negative pure imaginary solutions of k_N (blue curves in Fig. 4) correspondingly exist. Beyond the gap, the two OEMs can propagate in opposite directions without reflection in which the positive and negative real parts of k_N (Re(k_N)) exist (red curves in Fig. 4). All calculated values of the pure imaginary part of k_N (Im(k_N)) have been amplified four-fold. Moreover, the red curves (Fig. 4) indicate that the band gap blue-shifts from the long-wavelength (low-frequency) region to the short-wavelength (high-frequency) region as the oblique angle increases from 0° to 46°. Group velocity, v_g, can be defined as the slope of the dispersion relation of Re(k), such that [5],

$$v_g \equiv |d\omega / d(Re(k))| = c|d\omega_N / d(Re(k_N))|, \qquad (5)$$

According to Eq. (5), the red curves (Fig. 4(a)) indicate that the group velocities for the latter two OEMs approach zero ($v_g \rightarrow 0$) at the gap edges at each oblique angle, in which the corresponding wavelength at the LWE and SWE of the gap at each oblique angle is displayed in Fig. 4(b). According to the definition of DOS, the reciprocal of group velocity (DOS$\equiv 1/v_g$), the near null group velocity leads to a very large DOS (that is, DOS$\rightarrow \infty$) [8,10,12]. Therefore, the simulation results (Fig. 4) suggests that OEMs with wavelengths at the gap edges at each oblique angle have nearly null group velocity and infinite DOS. Figure 5 shows the
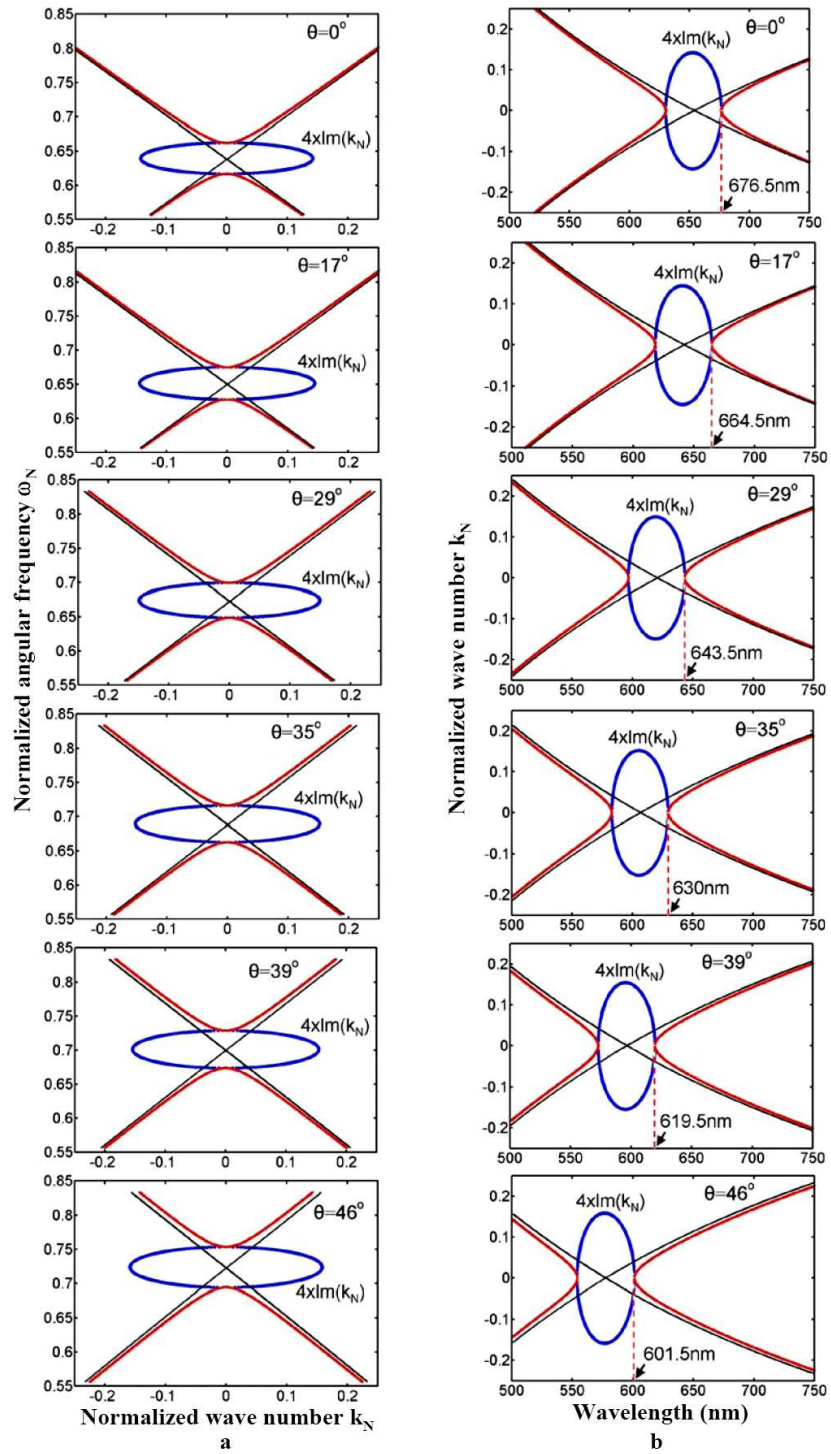
Fig. 4. Dispersion relation, (a) $\omega_N(k_N)$, or equivalently, (b) $k_N(\lambda)$, at different oblique angles $\theta=0$–$46°$ in a planar CLC structure. The parameters $\omega_N(\equiv\omega/(2\pi c/P))$ and $k_N(\equiv k/(2\pi/P))$ represent the normalized angular frequency and the normalized wave number of the incident optical eigenmodes (OEMs), respectively, where P is the pitch of the CLC.
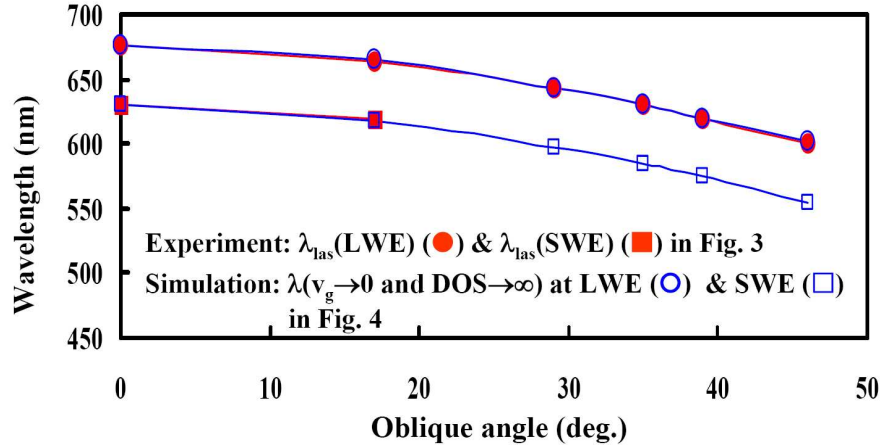
Fig. 5. The ● (■) and ○ (□) dots represent, respectively, the measured lasing wavelength at the LWE (SWE) of the CLC reflection band (λ_{las}(LWE) (λ_{las}(SWE)) in Fig. 3) and the simulated wavelength at the LWE (SWE) of the CLC stop band in which $v_g \to 0$ and DOS$\to\infty$ (λ($v_g \to 0$ and DOS$\to\infty$) at LWE (SWE) in Fig. 4) at different oblique angles.

comparison between variations of measured λ_{las}(LWE) (●) and λ_{las}(SWE) (■) and wavelengths at the LWE (○) and SWE (□) of the CLCRB in which $v_g \to 0$ and DOS$\to\infty$, which are obtained by simulation (Fig. 4(b)), with oblique angles. Experimental and simulation results are highly in agreement confirming that CCLE can be explained well based on photonic band-edge lasing theory for a distributed feedback resonator of a 1D PC-like planar DDCLC [5].

As presented in Figs. 2 and 3, the angular distribution of lasing intensity of the obtained CCLE occurred at the LWE is not uniform. This angular dependence of lasing intensity is related to variation in the energy threshold of the lasing emission in the CCLE with measured oblique angles. At each oblique angle, a corresponding energy threshold to lase exists (Fig. 6(a)), which is a natural sign for the occurrence of the lasing emission. The energy threshold at the six selected oblique angles ranked from high to low is $0° < 35° < 39° < 29° < 17° < 46°$ (Fig. 6(b)). The lasing emissions occurred at 0° and 35°, both of which have much lower energy threshold than those at other oblique angles; thus, they can be observed easily with the naked eye (Fig. 2(a)). Since the incident pumped energy used, 8.3μJ/pulse, is larger than the maximum energy thresholds, roughly 8.0μJ/pulse, measured at 46°, the CCLE (Fig. 2) can occur. To determine what causes result in the angular dependence of the energy threshold in the CCLE (Fig. 6(b)), another experiment measures the fluorescence and reflection spectra at the six oblique angles when pumped energy is reduced to 2.3μJ/pulse (near the minimum energy threshold measured at 0° (Fig. 6(b)). Figure 7 lists experimental data. The black, red, orange, pink, green and blue curves with peaks (notches) represent the measured fluorescence (reflection) spectra of the DDCLC at $\theta_1(\theta_2)=0°$, 17°, 29°, 35°, 39° and 46°, respectively. The fluorescence is strongly suppressed within the CLCRB, but enhanced only at the LWE of the CLCRB at each oblique angle. For off-normal cases, the magnitude of fluorescent peaks at the LWE measured at oblique angles increases from 17° to 35° as fluorescent intensity increases from 663.87 to 630.30nm in the gray fluorescence spectrum curve obtained when the cell is in an isotropic state. However, the decay of fluorescent intensity measured at large oblique angles (>35°) due to energy loss of the large angle reflection indicates that scattering of fluorescence may cause reducing the magnitude of fluorescent peak at the LWE as the oblique angle increases from 35° to 46°. The competition between the two angular dependent factors, the fluorescent spectrum distribution and the energy loss, therefore results in the angular dependences of lasing intensity and the energy threshold of the CCLE in the DDCLC.
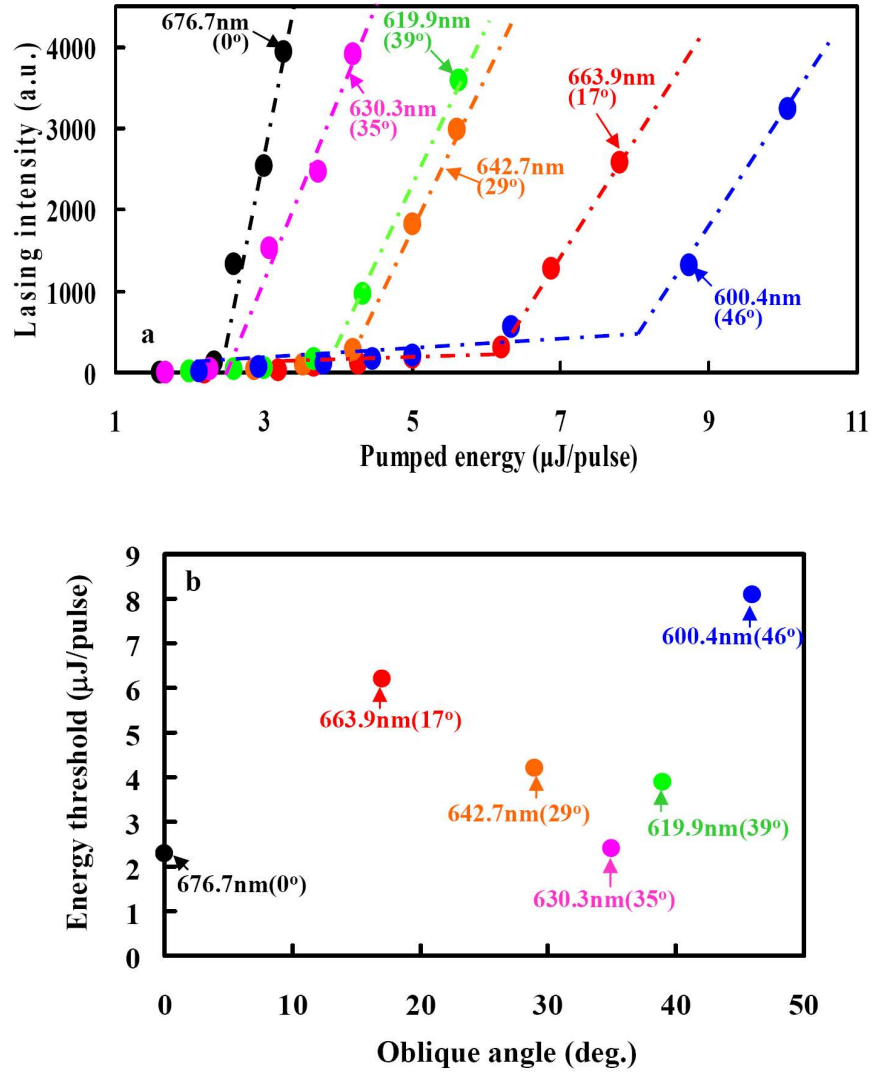
Fig. 6. (a) Variation of the lasing intensity of the CCLE (at the LWE) with the incident pumped energy at oblique angles of 0–46°. (b) Variation of the energy threshold of the CCLE with the oblique angle.
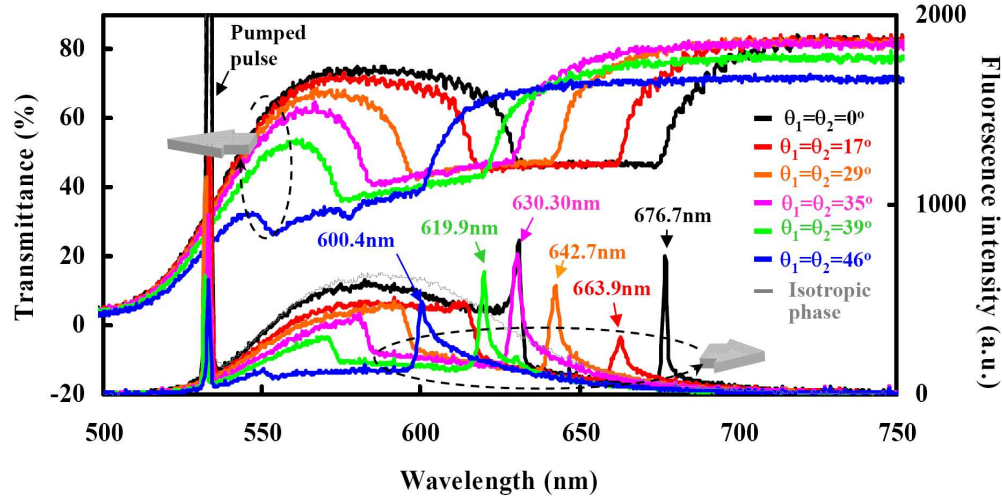
Fig. 7. Fluorescence and reflection spectra of the cell in CLC phase are measured at different oblique angles of $\theta_1=\theta_2=0$–46° when the cell is pumped by incident pulses with energy of 2.3μJ/pulse. The gray curve is the obtained fluorescence spectrum of the DDCLC cell in the isotropic phase measured at 0°.

4. Conclusion

In summary, an anomalous CCLE based on a 1D PC-like single-pitched DDCLC is first identified and investigated in this work. Experimental results reveal that this cell can lase simultaneously a wide-banded and conically symmetrical lasing emission, such that the lasing wavelength decreases as the cone angle increases. Simulation results using Berreman's 4×4 matrix method demonstrate that low-threshold edge lasing theory completely explains the angular dependence of the lasing wavelength of the CCLE at the LWE and SWE of the CLC stop band. Some peculiar features of the CCLE, such as the angular dependences of lasing intensity and the energy threshold are also identified and discussed. Forthcoming manuscripts will present experimental results that demonstrate the tunability of the CCLE lasing band and explain the mechanism for the formation of the anomalously strong lasing ring at 35° in the DDCLC.

Acknowledgments